

MASTER

TITLE: A NUMERICAL STUDY OF HOT-LEG ECC INJECTION
INTO THE UPPER PLENUM OF A PRESSURIZED WATER REACTOR

AUTHOR(S): Bart J. Daly (T-3)
Martin D. Torrey (T-3)
William C. Rivard (Flow Science, Inc)

SUBMITTED TO: Third CSNI Specialist Meeting on Transient
Two-Phase Flow
Pasadena, CA (CALTECH)
March 23-26, 1981

DISCLAIMER

By acceptance of this article, the publisher recognizes that the U.S. Government retains a nonexclusive, royalty-free license to publish or reproduce the published form of this contribution, or to allow others to do so, for U.S. Government purposes.

The Los Alamos Scientific Laboratory requests that the publisher identify this article as work performed under the auspices of the U.S. Department of Energy.

University of California



LOS ALAMOS SCIENTIFIC LABORATORY

Post Office Box 1663 Los Alamos, New Mexico 87545

An Affirmative Action/Equal Opportunity Employer

A NUMERICAL STUDY OF HOT LEG ECC INJECTION INTO
THE UPPER PLENUM OF A PRESSURIZED WATER REACTOR

Bart J. Daly and Martin D. Torrey
Theoretical Division, Group T-3
University of California
Los Alamos National Laboratory
Los Alamos, NM 87545

William C. Rivard
Flow Science, Inc.
Los Alamos, NM 87544

ABSTRACT

In certain pressurized water reactor (PWR) designs, emergency core coolant (ECC) is injected through the hot legs into the upper plenum. The condensation of steam on this subcooled liquid stream reduces the pressure in the hot legs and upper plenum and thereby affects flow conditions throughout the reactor. In the present study, we examine countercurrent steam-water flow in the hot leg to determine the deceleration of the ECC flow that results from an adverse pressure gradient and from momentum exchange from the steam by interfacial drag and condensation. For the parameters examined in the study, water flow reversal is observed for a pressure drop of 22-32 mBar over the 1.5 m hot leg.

We have also performed a three-dimensional study of subcooled water injection into air and steam environments of the upper plenum. The ECC water is deflected by an array of cylindrical guide tubes in its passage through the upper plenum. Comparisons of the air-water results with data obtained in a full scale experiment shows reasonable agreement, but indicates that there may be too much resistance to horizontal flow about the columns because of the use of a stair-step representation of the cylindrical guide tube cross section. Calculations of flow past single columns of stair-step, square and circular cross section do indicate excessive water deentrainment by the noncircular column. This has prompted the use of an arbitrary mesh computational procedure to more accurately represent the circular cross-section guide tubes.

1: INTRODUCTION

In certain pressurized water reactor (PWR) designs, emergency core coolant (ECC) is injected through the hot legs into the upper plenum. The condensation of steam on this subcooled liquid stream reduces the pressure in the hot legs and upper plenum and thereby affects flow conditions throughout the reactor. Thus, a systems code will be required to analyze the dynamics of this transient two-phase flow.

In the present study, we examine these steam-water flows in the hot leg and upper plenum in order to provide modeling assistance for the systems calculation. These component studies are now considered separately, although one objective of the program is to examine the interaction of the flow in the upper plenum with that in the hot legs.

In the hot leg part of the study, we assume that the ECC flow encounters an adverse pressure gradient that is driving steam counter to the water flow. We wish to determine the deceleration of the ECC flow that results from the adverse pressure gradient and from momentum exchange from the steam by interfacial drag and condensation. We have derived a computer model for the mass, momentum and energy exchanged in this countercurrent flow [1], based on the examination of a large body of experimental data dealing with cocurrent and countercurrent gas-liquid flow. We then examine the sensitivity of the steam-water interactions in the hot leg to variations in the coefficients of the mass and momentum exchange functions.

The effectiveness of the ECC system is enhanced if a large volume of this water can penetrate through the complex guide tube arrangement of the upper plenum to drain down and cool the central part of the core. Thus in the second phase of the study, we examine the breakup and deflection of the ECC jet by interactions with the guide tubes of the upper plenum and its loss of subcooling through the condensation of steam. In addition to the steam-water study, we also examine air-water interactions in the geometry of the upper plenum for comparison with full-scale experimental measurements [2].

In a Cartesian coordinate system it is necessary to represent the circular cross-section guide tubes by a stair-step arrangement of calculation cells. The sensitivity of the calculated results to the guide tube cross-sectional representation is examined by comparing results obtained in a single guide tube study using a stair-step, square or circular cross-section guide tube. These results suggest the need for a better guide tube representation, which is accomplished through the use of a computational procedure that permits an arbitrary mesh generation.

2: COUNTERCURRENT FLOW IN THE HOT LEG

In this study ECC is injected at the bottom of the hot leg from a pipe of roughly ellipsoidal shape. A schematic cross-sectional view of the hot leg and the ECC injection pipe is shown in Fig. 1. The cross-sectional area of the ECC

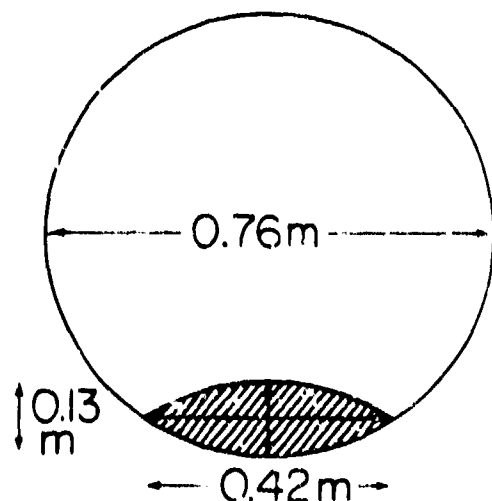


Fig. 1. A cross-sectional view of the hot leg pipe with the ellipsoidal ECC pipe at the bottom.

pipe is 0.038 m^2 , while that of the hot leg is approximately 0.45 m^2 . In the one-dimensional finite difference calculations we represent this two-phase pipe flow by two-phase flow in a rectangular channel, in which the lower 10% of the channel is filled with water and the upper 90% with steam, both at saturation temperature. Subcooled water (at temperature 308 K) is injected into the system through a port on the lower right side of the channel, at a velocity of -7 m/s . A pressure drop is maintained over the system, accelerating the steam counter to the water. The average pressure in the hot leg is about 6 Bars and the corresponding saturation tem-

perature is 431 K. The boundary conditions permit the steam flow to be reversed if the deceleration that results from momentum exchange with the water, together with wall drag, exceeds the pressure acceleration. However, the boundary conditions in this one-dimensional study do not permit water to be transported out across the water inlet end of the channel. If the water flow is halted before it reaches the outlet to the reactor vessel, the water accumulates in the channel in the form of a growing wave. We interpret this situation as effective water flow reversal and terminate the calculation. However, if the water penetrates to the reactor vessel, the calculation reaches a steady state condition. At steady state the water depth increases monotonically from the ECC inlet port to the reactor vessel, with the change in depth proportional to the water deceleration, so the mass flow rate is constant.

In this study we make use of a one-dimensional version of the K-TIF numerical method [3] for time-dependent, incompressible, multi-phase interactions. Reference 1 provides a description of the equations that are solved in this study, so that description will not be repeated here. However, we do discuss the momentum and mass exchange functions that are used.

The interfacial momentum exchange function has the form

$$K = f_w \rho_g |u_l - u_g| / H \quad , \quad (1)$$

where ρ is density, u is velocity, H is the height of the calculation region, and the subscripts g and l refer to gas and liquid. The coefficient f_w accounts for the waviness of the interface, and corresponds to the ratio of wave amplitude to wavelength [1]. For the relative velocities that exist in this study we expect to encounter three wave regimes: three dimensional waves, roll waves and droplet entrainment from unstable wave crests. Transitions between flow regimes appear to be scale dependent [1], but in large scale horizontal air-water experiments Wallis [4] determined that three dimensional waves develop at a relative velocity of about 5 m/s, the transition to roll waves occurs at about 11 m/s, and entrainment begins at about 17 m/s. In other large scale experiments van Rossum [5] determined that the relative velocity for water droplet entrainment in air is about 18 m/s.

In the hot leg injection study we assume that the momentum exchange coefficient f_w varies with flow regime, using Wallis' relative velocity criteria for the transitions between flow regimes. We express this assumption,

$$f_w = f_{w \max} \times \begin{cases} 0.1 , & u_{rel} < 5 \text{ m/s} \\ 0.1 + 0.033(u_{rel} - 5) , & 5 < u_{rel} < 11 \text{ m/s} \\ 0.3 + 0.117(u_{rel} - 11) , & 11 < u_{rel} < 17 \text{ m/s} \\ 1.0 , & 17 < u_{rel} \end{cases} \quad (2)$$

where $u_{rel} = |u_l - u_g|$. Interpreting f_w as the ratio of wave amplitude to wavelength, the relations in Eq. (2) imply that the ratio is $0.1 f_{w \max}$ at the on-

set of three dimensional disturbances, $0.3 f_{\omega \max}$ at the onset of role waves, and $1.0 f_{\omega \max}$ in the droplet entrainment regime. The droplet entrainment regime does not correspond to a particular wave form, but the increase in the momentum exchange coefficient for this regime derives from the assumption that the addition of droplets to the gas field results in increased interfacial drag. One could also consider modifying the density of the gas field to account for droplet entrainment, but this was not done in this study.

The mass per unit volume per unit time changing phase by condensation is given by

$$J = J_c \frac{\rho_l b}{h_{fg} H} s_l |u_g - u_l| \frac{T_g - T_l}{d} \quad (3)$$

in the hot leg study. Here J_c is a nondimensional coefficient, b is specific heat, h_{fg} is latent heat, s is the turbulent macroscale, T is the temperature and d is the thermal boundary layer thickness. The principal factor controlling mass exchange at the interface is the turbulent mixing of cool water from within the liquid layer up to the interface. We include this effect in Eq. (3) by the product $s_l |u_g - u_l|$, which is proportional to a turbulent eddy viscosity. The ratio of length scales s_l/d in Eq. (3) is modeled by

$$\frac{s_l}{d} = \left(\frac{x}{L} + 10^{-4} \right)^{-\frac{1}{2}} \quad (4)$$

where x/L is the fractional distance measured from the ECC inlet port. The purpose of this form is to represent a very thin thermal boundary layer at the ECC injection port and the rapid growth of this boundary layer with distance from this inlet. The model has not been tested experimentally and hence could be a source of excessive heat transfer to the water in this study.

We estimate the magnitude of the mass exchange coefficient J_c on the basis of numerical comparisons with small scale condensation experiments performed at Northwestern University [6]. A value $J_c = -4 \times 10^{-4}$ gave good agreement with experiments in one-dimensional calculations of those cocurrent, horizontally-stratified steam water flows.

The wall friction coefficients for the water and steam were obtained from Schlichting [7], assuming a sand roughness value equivalent to that of structural steel pipe. The coefficients used in this study are $c_1 = 0.014$ and $c_2 = 0.011$. The larger friction coefficient for the water reflects the fact that, prior to entry into the hot leg, the water had been flowing in a much smaller pipe. In the numerical computations the friction coefficient for the steam is multiplied by an area ratio factor to account for the greater surface area of interaction in hot leg pipe compared to the rectangular calculation region. No such adjustment is applied to the water, because its area of interaction is approximately the same in both cases.

2.1. Results of the Calculations

The principal uncertainties in this calculational study are the coefficients of the mass and momentum exchange functions, J_c and f_w . Therefore in this section we examine the sensitivity of the steam-water interactions to variations of these coefficients. We also examine the important interactions between the condensation process and the pressure variations in the system, and the consequences of these interactions on momentum exchange between the phases.

Figures 2 and 3 show some results of variations in the mass exchange coefficient J_c . Figure 2 shows the calculated water velocity at the exit to the reactor vessel as a function of pressure drop over the 1.5 m channel. Each datum point represents a steady-state result obtained from a single numerical calculation. The water, which is injected into the hot leg at the velocity - 7 m/s, is decelerated during flow through the 1.5 m channel by the adverse pressure gradient and by momentum exchange from the steam and from the rigid wall. Increasing the pressure drop increases the deceleration, so that the results take the form of a flooding curve, with increased pressure drop leading to decreased water penetration velocity and finally to zero penetration, or complete flooding.

The value $J_c = -4 \times 10^{-4}$ was found to produce good agreement with experiment [6] in a one-dimensional numerical study of cocurrent, horizontally-stratified, steam-water flow. Thus, in the absence of other information, this is our best estimate of the value of J_c . However, Fig. 2 shows that a variation of this coefficient from 0 to 1.2×10^{-3} has relatively little effect on the water exit velocity into the reactor vessel. The minimum sustainable exit velocity is approximately -2.5 m/s; any greater deceleration results in water flow reversal. For the range values of J_c examined in Fig. 2, flow reversal occurs for a pres-

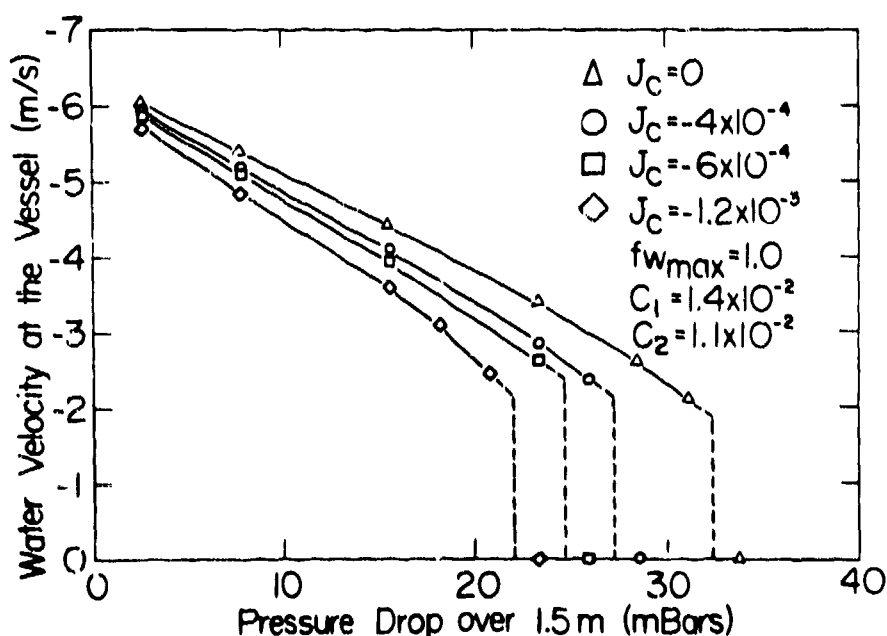


Fig. 2. Water velocity at the exit from the hot leg to the reactor vessel as a function of pressure drop over the 1.5 m channel for four values of the mass exchange coefficient.

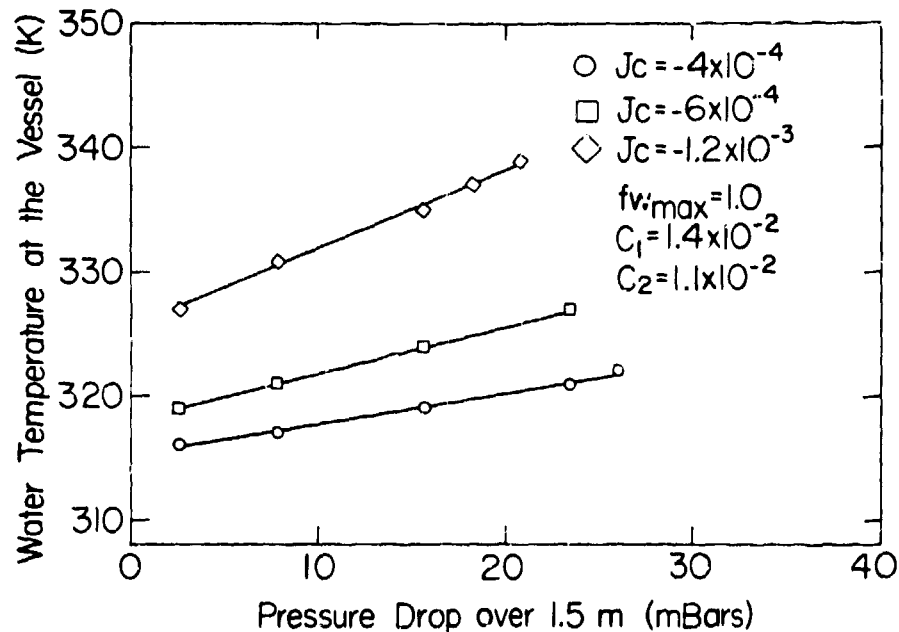


Fig. 3. Water temperature at the exit from the hot leg to the reactor vessel as a function of pressure drop over the 1.5 m channel for three values of the mass exchange coefficient. The water is injected into the hot leg at the temperature 308 K, and the saturation temperature is 431 K.

sure drop from the vessel to the ECC inlet of approximately 22-32 mBar over this 1.5 m distance.

The principal effect of condensation on momentum exchange in the hot leg comes about, not through phase change, but through the greater interfacial drag that results from the increase in the steam velocity into the channel. The largest inlet steam velocity against which water can penetrate into the reactor vessel is about 21 m/s for the four values of J_c considered in Fig. 2.

The water temperature at the exit to the reactor vessel increases with the mass exchange coefficient J_c and with the pressure drop over the hot leg, as shown in Fig. 3. The water enters the hot leg at 308 K, so these results indicate a decrease in subcooling in the range 8-31 K for the three values of J_c considered. Of course, when $J_c = 0$ the water remains at the initial subcooling of 123 K. Two factors that contribute to the increase in water temperature with pressure drop are the increase in the relative velocity between the fluids, which leads to greater turbulent mixing in the water layer and hence more condensation, and the longer residence time of the water in the channel.

In Fig. 4 we examine the sensitivity of the calculated steam-water flow in the channel to variations of the momentum exchange coefficient $f_{w \max}$ of Eq. (2). Figure 4 shows flooding curves of the water velocity at the exit to the reactor vessel as a function of the pressure drop over the channel for three values of $f_{w \max}$. The exiting water velocity is not strongly sensitive to

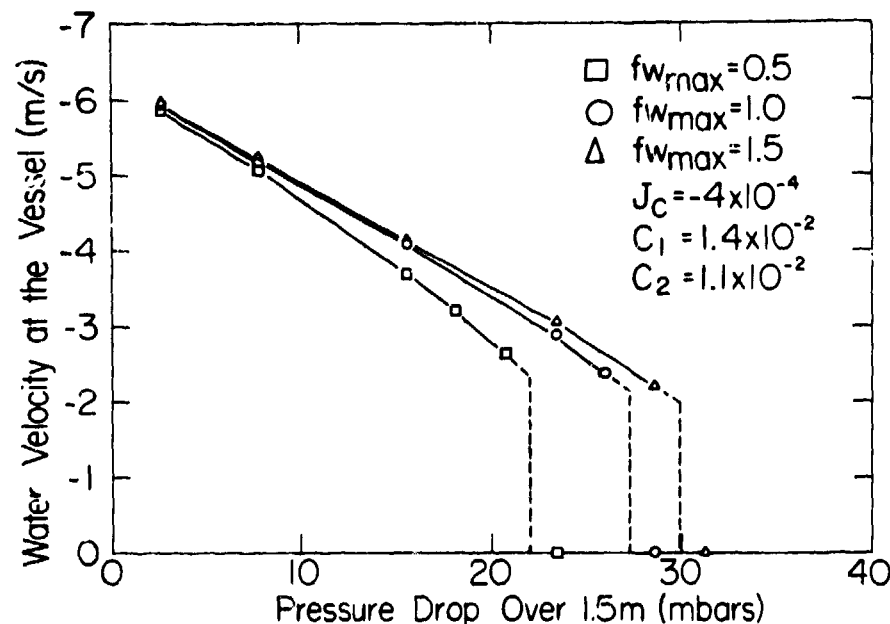


Fig. 4. Water velocity at the exit from the hot leg to the reactor vessel as a function of pressure drop over the 1.5 m channel for three values of the momentum exchange coefficient in Eq. (2).

$f_{w \max}$ when plotted in this way. However, these results indicate that this water velocity increases with $f_{w \max}$ for a given pressure drop. While this result appears counter-intuitive it can be explained by the relationship between condensation and interfacial drag.

When the drag coefficient is decreased at a given pressure drop, the calculated steam flow into the channel is increased. In the absence of condensation, the steady-state interfacial drag is changed only slightly, because the pressure gradient and the interfacial drag term dominate the gas momentum equation under these circumstances. If the drag coefficient is decreased, the gas velocity into the system will increase, so that the pressure gradient and interfacial stress will again be in balance. Thus, there will be a greater relative velocity between the fluids, so if condensation is included, as it was in the calculations of Fig. 4, there will be more momentum exchange by that mechanism [see Eq. (3)]. Hence, the calculated water flow into the reactor vessel decreases with decreasing $f_{w \max}$ at a given pressure drop over the channel.

For the range of values of the coefficient $f_{w \max}$ considered in Fig. 4, the pressure drop over the channel required for flow reversal varies in the range 22-30 mBar. The minimum sustainable water velocity into the reactor vessel is approximately -2.5 m/s. The maximum incoming steam velocity for which water is able to penetrate into the reactor vessel varies from about 17 m/s when $f_{w \max} = 1.5$ to about 30 m/s when $f_{w \max} = 0.5$.

In Fig. 5 we show the variation in the water temperature at the exit to the reactor vessel for the range of parameters examined in Fig. 4. The water temperature shows an opposite trend from that of the water velocity data for

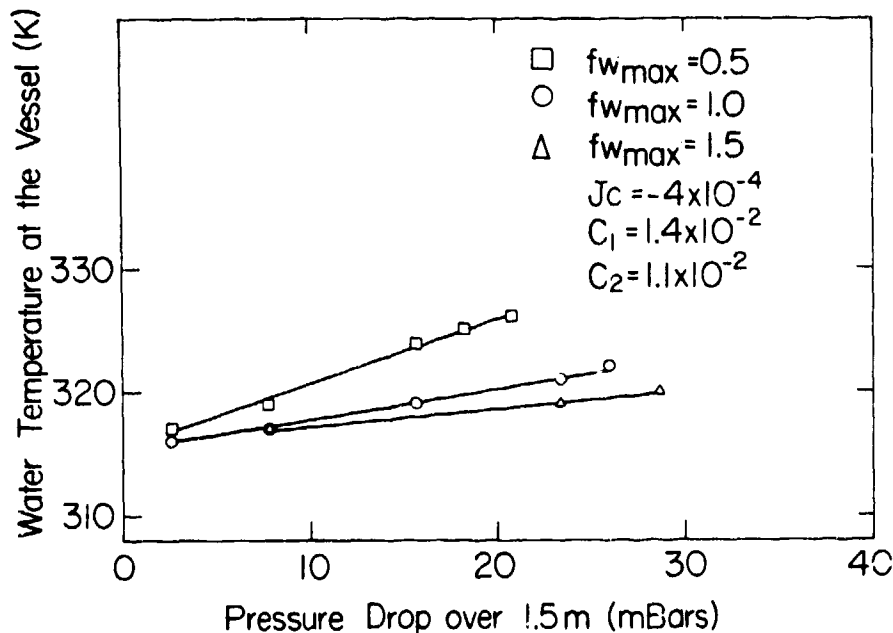


Fig. 5. Water temperature at the exit from the hot leg to the reactor vessel as a function of pressure drop over the 1.5 m channel for three values of the momentum exchange coefficient in Eq. (2). The water is injected into the hot leg at the temperature 308 K, and the saturation temperature is 431 K.

the reasons discussed in relation to Fig. 3. A decrease in $f_{w \max}$ or an increase in the pressure drop causes an increase in the relative velocity between the fluids, which promotes greater turbulent mixing within the water layer and hence more condensation and heat transfer from the steam, and an increase in the water residence time in the channel.

2.2. Validity of the Results

The validity of these results might well be questioned on the basis of uncertainty in the values of the mass and momentum exchange coefficients used in the numerical calculations. However, Fig. 2 indicates that these results are not very sensitive to the value of the mass exchange coefficient within a reasonable range of its variations. Indeed, the main conclusion would be the same if we neglected condensation entirely. However, there may be a greater uncertainty in regard to the value of the momentum exchange coefficient used in this study, although the results of Fig. 4 indicate that a further decrease in the momentum exchange coefficient from those considered here may result in ECC flow reversal at even smaller pressure drops.

There is another way of checking on the results of this study without regard to the form of the mass and momentum exchange terms. This can be done by considering the mixture equation formed by adding the steady state momentum equations and neglecting axial diffusion and wall drag. Using this procedure, it is shown in reference 1 that a pressure drop over the hot leg of 23.3 mBar

would produce a 50% decrease in water velocity in the hot leg. This is consistent with the results of Figs. 2 and 4.

3: DEFLECTION OF THE ECC JET BY UPPER PLENUM COLUMNS

In the upper plenum study we will consider both air-water and steam-water interactions. The results of the air-water study are compared with measurements obtained in a three-dimensional, full-scale test facility in Germany [2]. Figure 6 shows a horizontal cross section of the test facility and outlines a subsection of the upper plenum for which numerical computations were performed. Also shown in the figure is the hot leg and the ECC injection pipe which lies on the bottom of the hot leg as shown in Fig. 1.

In the air-water experiments [2] water was injected into the upper plenum from the hot leg opening at the rate 333 kg/s (inlet velocity is 7.9 m/s) at atmospheric pressure. Pitot tube measurements were made 106 cm below the water injection elevation. The pitot tube resided in a water pool 1 cm below the pool surface and was moved along the line-of-sight paths between the columns. The recorded pressure head at numerous locations was used to deduce information on the vertical flow rate. Around the perimeter, between the outer columns and the plenum wall, flow rate data was taken with a pair of cups that could be moved along arcs of constant radius. The cups were located 172 cm below the water injection elevation.

3.1. Calculations in a Cartesian Coordinate System

The three dimensional K-FIX code [8] has been used to perform both air-water and steam-water calculations in this upper plenum geometry. Since this code is fully documented we will not describe it here, but we do discuss the momentum and mass exchange terms used in the study.

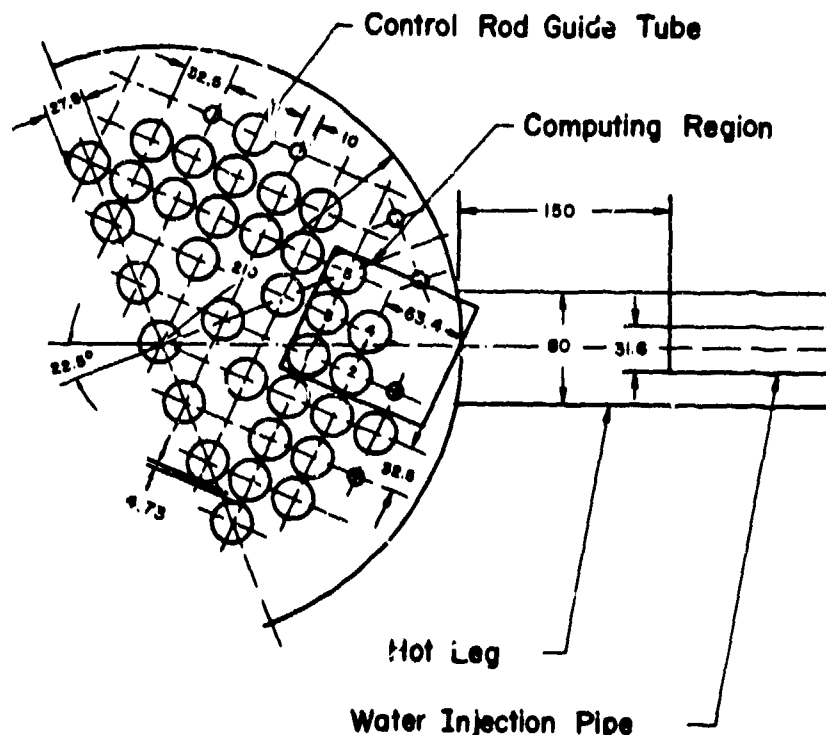


Fig. 6. Horizontal section of the air-water test facility and the computing region boundaries. Dimensions are in cm.

The momentum exchange function has the form

$$K = \frac{3}{4} \rho_g \{ \alpha(1-\alpha) |u_l - u_g| + \nu / [r\alpha(1-\alpha)] \} / r, \quad (5)$$

where r is a mean entity size and ν is the kinematic gas viscosity. The first group of terms in Eq. (5) describes the momentum exchange function that is effective for nonvanishing values of the volume fractions, while the second group ties the two fields together near the volume fraction limits. Although the latter is probably too restrictive on the droplet motion, only very small amounts of the injected water are involved, since void fractions typically greater than 99% are required to significantly reduce relative motion. The form of Eq. (5) is equivalent to that used in PWR downcomer studies [9], which involved highly agitated gas-liquid interactions such as observed during upper plenum injection. The entity size r was taken to be about twice the value used for the downcomer study because of the more cohesive appearance of the water flow. On this basis we obtain the value $r = 0.24$ cm.

The mass exchange function used in the steam-water calculations is equivalent in form to that of Eq. (3), but the coefficient now is proportional to the product of the volume fractions, and the term H is replaced by a factor proportional to the cell size. The turbulent macroscale and the thermal boundary layer thickness are assumed to be $1/4$ and $1/2$ the spacing between the upper plenum guide tubes, respectively. The final mass exchange rate is 20% smaller than that used in downcomer flow simulations [9].

In the horizontal plane the computing region is a mesh of 19×23 square cells, 5 cm on a side. The circular guide tubes are approximated with 13 of these cells, as indicated in Fig. 7, which shows the steady-state liquid velocity field in the air-water calculation at the water injection elevation. Five

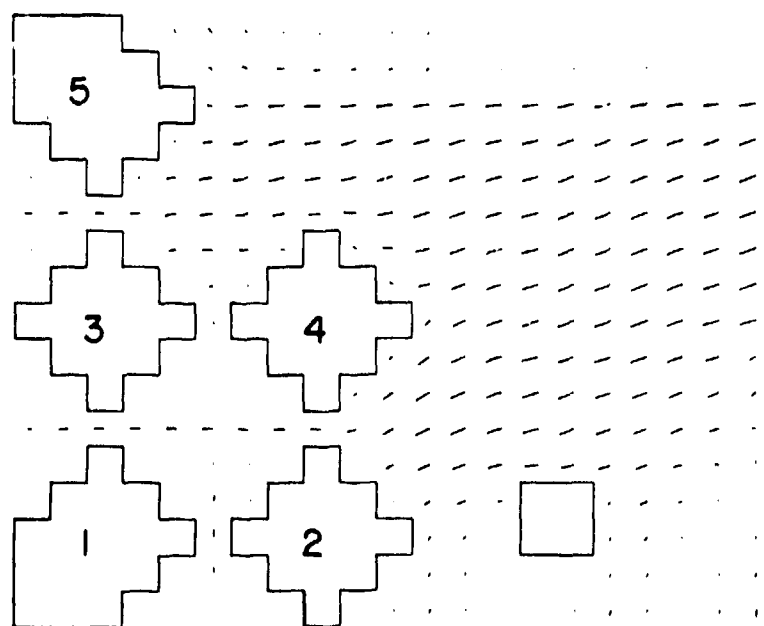


Fig. 7. Steady-state liquid velocity field for the air-water calculation at the elevation of the water injection. The speed of the incoming water is 790.4 cm/s.

major guide tubes and one minor one are resolved in the numerical study. In the vertical direction there are 17 computation cells, each 13.05 cm high.

Results of the calculations. The comparison of the air-water calculation data and the comparisons of the steam-water and air-water results are shown in Figs. 8-11. Figure 8 shows the flow rate distribution in kg/s for water leaving the computing mesh across its bottom boundary. The values represent averages over the indicated regions. Values in parenthesis correspond to the data, while the others are calculated results. The total water flow across the bottom, which is the sum of the flow in each region, is calculated to be 131 kg/s compared with a value of 80 kg/s indicated by the data. In the regions around the columns, where the calculated averages are significantly higher than the data, large contributions to the average occur from the cells adjacent to the columns, which indicates film flow down the columns. Such a situation could not be accurately measured by the pitot tube transversing between the columns. At best the pitot tube could detect only the induced wave motion on the water surface, but any inference about the vertical flow rate from a Bernoulli relation, as is done, would be an underestimate. On the other hand, the stairstep approximation to the circular cross-section of the columns used in the calculational model offers more resistance to horizontal flow than it should. This point will be considered in more detail below.

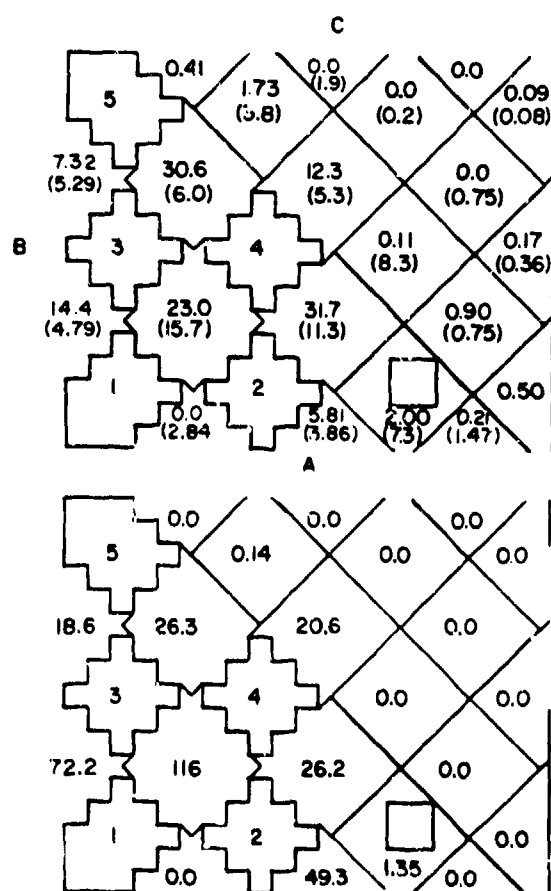


Fig. 8. Flow rate distribution in kg/s for water flowing out of the computing mesh across its bottom boundary for the air-water (upper) and steam-water (lower) calculations.

The water flow across the bottom for the steam-water calculation is greater than for air-water. The total flow is 331 kg/s, which is very nearly equal to the water injection rate. (Note: No account is taken of any deceleration or warming of the ECC flow in the hot leg. We assume that it enters the upper plenum at its initial velocity and subcooling.) A considerable mass flow rate of steam enters the computing mesh through the open vertical sides. No steam enters through the bottom in accordance with the boundary condition used for the air-water calculation. The flow rate of steam that enters the computing region and condenses to water is 26 kg/s. The entering steam brings with it entrained droplets that amount to 25 kg/s, so that the total water influx to the computing region is 358 kg/s. When this inflow rate is added to the 26 kg/s, produced internally from condensation, it balances the net outflow rate of 384 kg/s at steady state, which is achieved at about 1.4 s. About 35% of the injected water flows across the bottom of the computing mesh just behind the lead column. Large amounts of condensation occur as the jet collides with the lead column because of the

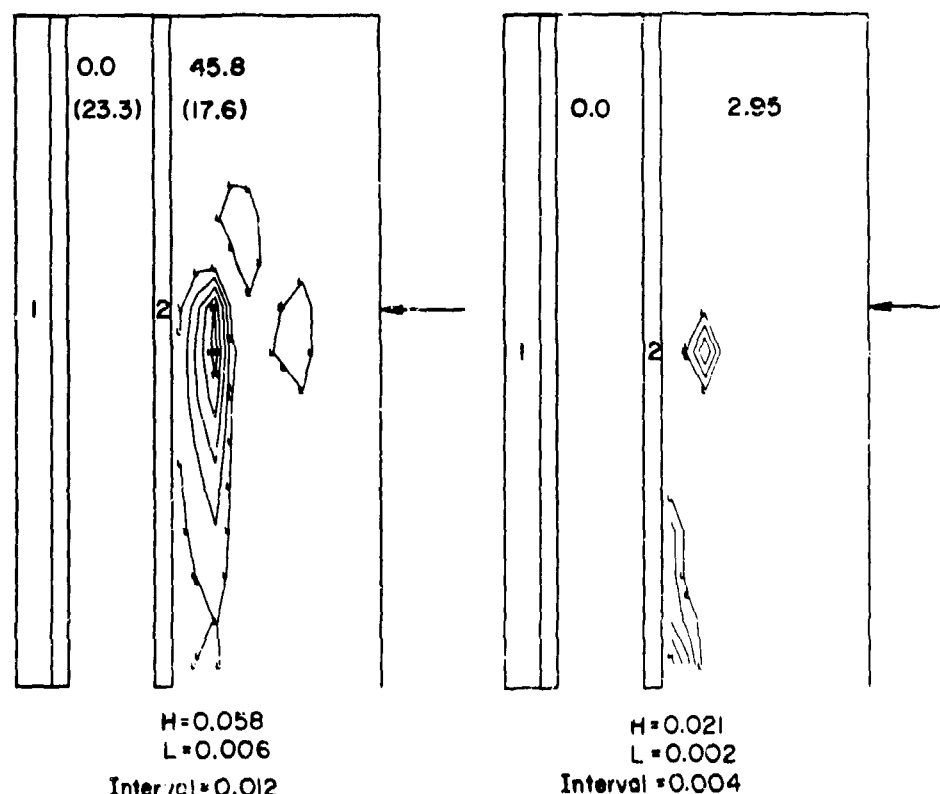


Fig. 9. Contours of mass flux in $\text{kg/s}\cdot\text{cm}^2$ flowing across vertical face A (see Fig. 8) for the air-water (left) and steam-water (right) calculations. The values shown between the columns are flow rates in kg/s . Those in parenthesis are the data values.

significant increase in the steam-water contact area. The momentum transfer from condensation and the frictional resistance of the countercurrent flowing steam rushing toward the initial impact point dissipate the horizontal momentum of the water jet.

The water flow across the vertical boundaries of the computing mesh are shown as contours of mass flux ($\text{kg/s}\cdot\text{cm}^2$) in Figs. 9-11 for faces A, B, and C (see Fig. 8), respectively. The left-hand plot in each figure shows values for the mass flow rate between the columns calculated for the air-water tests, compared with the data shown in parentheses. The right-hand plot shows the corresponding steam-water results. The arrows on each plot denote the elevation of the water injection port centerline. In Fig. 9 (face A) the calculated total water outflow of 45.8 kg/s agrees well with the total measured rate of 41.0 kg/s ; however, the calculated distribution across the face is different from that measured. The steam flow rate across this face is negligible.

On face B (Fig. 10), which is the most important face for considerations of core cooling efficiency, agreement with the data for the flow rate between columns 1 and 3 is very good. The calculated flow rate between columns 3 and 5, however, is only about one-half the data value. The loss of water flow between these columns is essentially equal to the excess flow calculated across

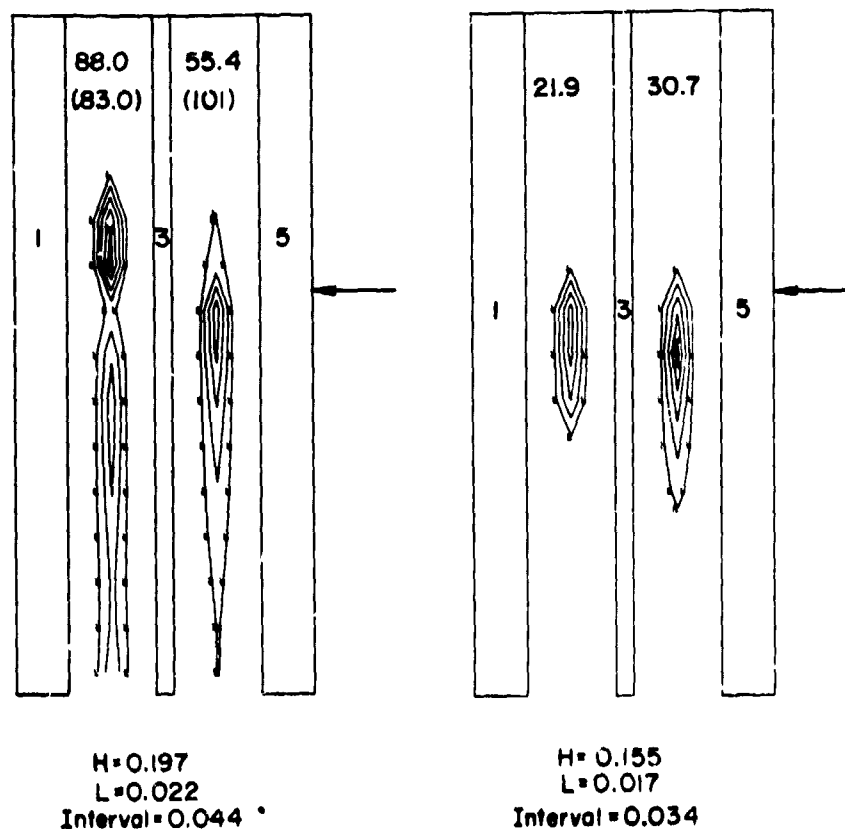


Fig. 10. Contours of mass flux in $\text{kg/s}\cdot\text{cm}^2$ flowing across vertical face B (see Fig. 8). The orientation of the plots and the meaning of the values is the same as in Fig. 9.

the bottom. The flow rates for steam-water are much lower than for air-water and the sheet structure of the flow is reduced.

The flow rate across face C in Fig. 11 is the smallest flow crossing the vertical boundaries. This calculated flow is highly voided and, although the exiting region is large, the flow rate is low (11.5 kg/s). The data indicate twice as much water to be exiting but the highly-voided description and the exit location agree with the observations. In the steam-water calculation no water leaves the computing mesh across the boundary. In fact, the incoming steam flow brings with it as entrained droplets about 19 kg/s of water.

The water injection temperature is 293 K, which is 130°C subcooled at 6 mBars. The water is heated only by latent heat deposition from condensation. No heat transfer with the columns is considered. The temperature of water crossing the bottom of the computing mesh varies from 301 K to 366 K, with a mean of about 325 K, which is 107°C subcooled. The temperature of water crossing faces A and B is somewhat higher. For face A the temperature ranges from 307 K to 421 K, but only a small amount of water is involved. For face B the temperature ranges from 306 K to 416 K with most of the water at about 374 K, which is 58°C subcooled.

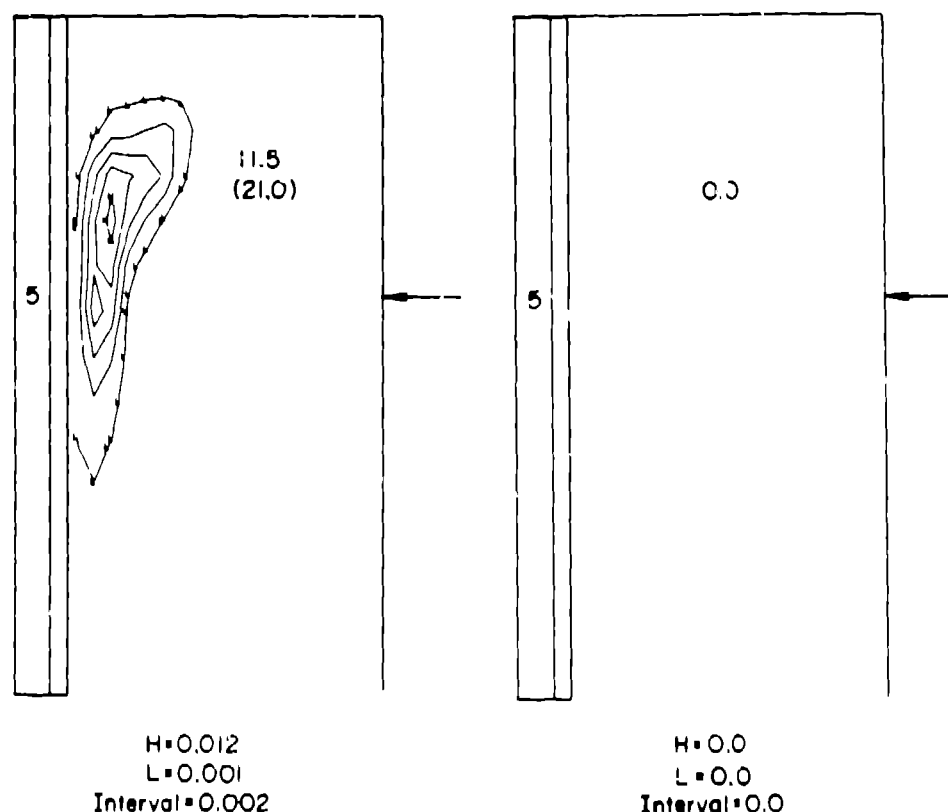


Fig. 11. Contours of mass flux in $\text{kg/s}\cdot\text{cm}^2$ flowing across vertical face C (see Fig. 8). The orientation of the plots and the meaning of the values is the same as in Fig. 9.

3.2. The Effect of Guide Tube Cross Section on Momentum Flux.

In the previous section we saw that the numerical results showed a greater liquid flow rate through the bottom boundary of the computation region, and correspondingly less flow through the sides, than was deduced from the experiment. A possible explanation for this is that there is an excess transfer of horizontal to vertical momentum as a result of using a stair-step representation of the circular guide tubes. This explanation is supported by the observation that the calculational cells that show the greatest vertical liquid mass flow are located on the front face of the columns.

To test the theory that the use of a stair-step representation of a round cylindrical column will result in excess transfer of horizontal to vertical momentum we have performed a study of water flow past a single cylindrical column of stair-step, square and circular cross section in an air environment. The calculation of flow past a circular cylinder was performed in cylindrical coordinates, while the other calculations made use of a Cartesian coordinate system. In all cases the liquid flow enters the computation region from the upper right boundary at a velocity of approximately 6.7 m/s . The cross-sectional areas of the square and cylindrical columns are approximately equal, while the stair-step column corresponds to the square column with three computation cells deleted from each corner. The effect of these variations in column cross section on the liquid mass flux through the bottom boundary of the computation mesh can be seen in Fig. 12. For the stair-step cross-section column most of

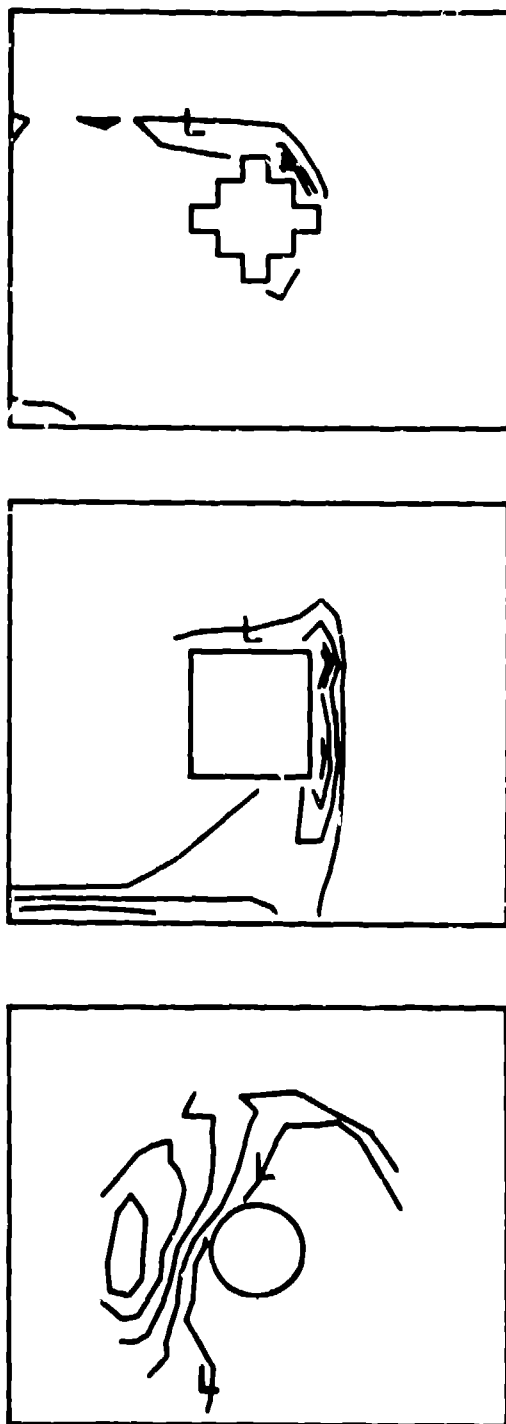


Fig. 12. Contours of liquid mass flux through the bottom boundary from calculations of air-water flow past stair-step (top), square (middle) and circular (bottom) cross-section columns.

the liquid flux is concentrated in the stair-step region in one corner of the column. This is consistent with the observations of section 3.1. In the square column calculation the vertical liquid flux is more uniformly distributed along the front face of the obstacle. In the calculation of flow past the circular cylinder the vertical liquid mass flux is much more uniformly distributed, with the maximum occurring in the wake of the obstacle. The total liquid mass fluxes through the bottom boundary of the calculation region in kg/s are 53.4, 59.7 and 35.1 for the stair-step, square and cylindrical columns, respectively. This result demonstrates that the use of stair-step or square cross-section columns results in much greater vertical liquid flow in the immediate vicinity of the column than is seen in the calculation of flow past a circular cylinder.

3.3. Calculations in an Arbitrary Coordinate System

In order to improve our ability to resolve circular cross-section columns we are now using the SALE-3D computational procedure [10] in these upper plenum studies. This method permits a completely arbitrary mesh arrangement and thereby permits us to more nearly represent the circular cross-section of the columns, as shown in Fig. 13. This figure shows a cross-sectional view of a mesh generated to represent one-half of the upper plenum as shown in Fig. 6. The columns are represented in cross section by octagons, and the regions between the columns are smoothly zoned to minimize computational difficulties.

Figures 14 and 15 show some preliminary results obtained in applying this procedure to the hot leg ECC injection study. These figures show a velocity plot and a void fraction contour plot at the elevation of ECC injection for a steam-water calculation. The figures show two hot leg

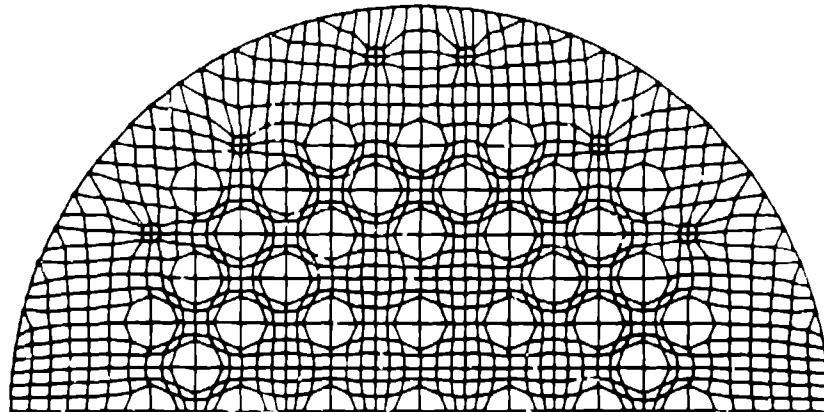


Fig. 13. A horizontal cross-section of the calculation mesh used in the SALE-3D upper plenum study.

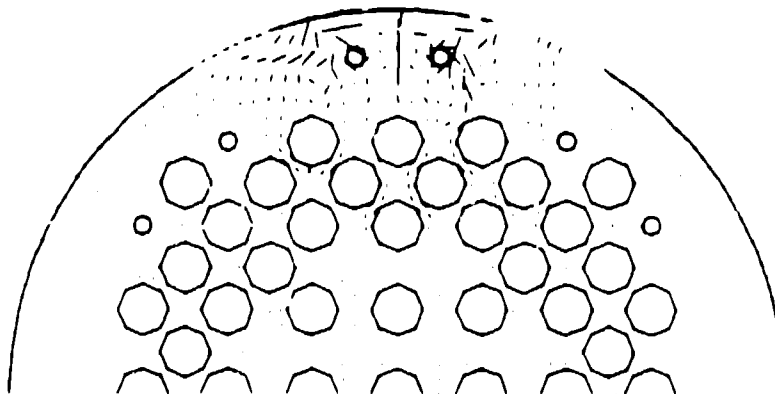


Fig. 14. A velocity vector plot at the elevation of water injection from a steam-water upper plenum calculation using SALE-3D.

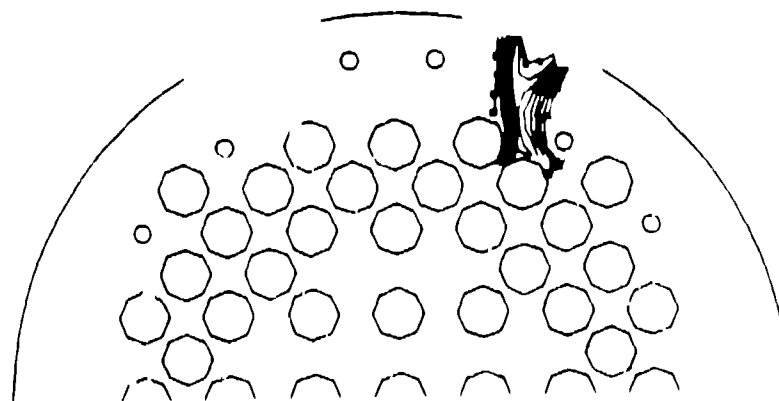


Fig. 15. A void fraction contour plot at the elevation of water injection from a steam-water upper plenum calculation using SALE-3D.

openings, but the opening on the left is closed off and treated as a free-slip wall in this calculation. In this study we use a homogeneous procedure for the calculation of fluid motion, so the velocity plot shows both gas and liquid motion. The incoming water jet has generated vortices in the steam field near the inlet region and there is gas motion as well in the regions between the

guide tubes. The void fraction plot shows that the liquid jet has been deflected, possibly through the action of the steam vortices. This liquid distribution appears to be consistent with the steam water results seen in the K-FIX calculations of Fig. 8.

4: Conclusion

In the hot leg part of this study we have examined a horizontally stratified steam-water flow in a pipe leading to the upper plenum of a pressurized water reactor. For a wide range of variations in the mass and momentum exchange coefficients we observe a very similar pattern of ECC deceleration as a function of pressure drop over the hot leg. For the parameters examined, water flow reversal occurs for a pressure drop in the range 22-32 mBar over the 1.5 m hot leg.

We have also studied the effects of injecting subcooled ECC water into air and steam environments in the upper plenum of a PWR. In addition to the multiphase interactions that occur in this study, it is also necessary to calculate the passage of the water through a complex array of guide tubes. The air-water results are in reasonable agreement with experimental measurements, but they indicate that there may be too much resistance to horizontal flow about the columns because of the stair-step shape of the column cross section. Calculations of flow past single columns of stair-step, square and circular cross section indicate that the noncircular columns deentrain more water than the circular column. Furthermore, this deentrainment occurs on the front face of the column, while in the circular case most of the deentrainment occurs in the wake of the columns.

These results suggest that improved accuracy of upper plenum flow simulations could be obtained if the circular cross section of the guide tubes was modeled more accurately. This has prompted the use of a computational procedure that allows an arbitrary mesh arrangement to more nearly represent the circular cross section.

ACKNOWLEDGMENTS

This work was performed under the auspices of the U.S. Nuclear Regulatory Commission.

REFERENCES

1. B. J. Daly and F. H. Harlow, A Model of Countercurrent Steam-Water Flow in Large Horizontal Pipes, Nucl. Sci. and Eng., Vol. 77, pp. 273-284, 1981.
2. H. Kiehne, Luft-Wasser-Versuche in Oberen Plenum, Kraftwerk Union report R-11-1002-79, West Germany, 1979.
3. A. A. Amsden and F. H. Harlow, K-TIF: A Two-Fluid Computer Program for Downcomer Flow Dynamics, Los Alamos National Laboratory report LA-6994, Los Alamos, N.M., Jan. 1978.
4. G. B. Wallis, Two-Phase Flow and Boiling Heat Transfer, Joint U.S. - Euratom Research and Development report NYO-3114-14, Jan. 1966.
5. J. J. van Rossum, Experimental Investigation of Horizontal Liquid Films, Chem. Eng. Sci., Vol. 11, pp. 35-52, 1959.

6. S. G. Bankoff, R. S. Tankin and M. C. Yuen, Condensation Rates in Steam-Water Mixing, Northwestern University annual progress report to the U.S. Nuclear Regulatory Commission, Evanston, IL, 1979.
7. H. Schlichting, Boundary-Layer Theory, 7th ed., Figs. 20.25 and 20.26, McGraw-Hill Book Co., New York, 1979.
8. W. C. Rivard and M. D. Torrey, K-FIX: A Computer Program for Transient, Two-Dimensional, Two-Fluid Flow; THREED: An Extension of the K-FIX Code for Three-Dimensional Calculations, Los Alamos National Laboratory report LA-NUREG-6623, Suppl. II, Los Alamos, N.M., April 1977.
9. B. J. Daly, The Sensitivity of Emergency Core Coolant Bypass and Lower Plenum Refill to Apparatus Scale Size and Lower Plenum Pressure in a Pressurized Water Reactor, Nucl. Sci. Engr., Vol. 72, pp. 97-107, 1979.
10. A. A. Amaden and H. M. Ruppel, SALE-3D: A Simplified ALE Computer Program for Calculating Three-Dimensional Fluid Flow, Los Alamos National Laboratory report to be published, Los Alamos, N.M.